



Cite this: *Environ. Sci.: Water Res. Technol.*, 2023, 9, 833

Empowering clean water whilst safeguarding water distribution pipeline integrity: towards manganese- and iron-free lime hydrate for water treatment†

Dávid Kocsis,^{*abc} Rhys A. Ward,^{bc} Christopher R. Meyer,^{*a} Michael Thompson,^d Timothy J. Prior, ^d Stephen M. Kelly, ^{cd} Nathan S. Lawrence ^{bc} and Jay D. Wadhawan ^{*bc}

Hydrated limes are amongst the most economically valuable alkalis used by the water industry for the treatment of potable water. They are typically manufactured from the thermal decomposition of high purity limestones. However, the latter contain both manganese and iron impurities, which are transformed into the oxides Mn_3O_4 and Fe_2O_3 on burning in kilns (between 900–1100 °C) during the manufacture of lime, and are retained in the lime hydrate upon slaking. These impurities can be released through oxidation by conventional water disinfection chemicals (such as alkaline hypochlorite) during the use of lime hydrate as the alkaline pH modifier during conventional operations in water treatment works. This work investigates the redox mechanisms for manganese and iron removal from lime hydrate using alkaline hypochlorite: for manganese, interfacial electron transfer occurs first leading to dissolution as permanganate; in the case of iron impurities, solubility is encouraged in oxygenated solutions first through formation of solid ferrite, with oxidative dissolution of ferrite to ferrate. As expected for activation-controlled reactions, the oxidative dissolution is enhanced with increased temperatures; mapping the dissolution process with time allows for the unravelling of “rule-of-thumb” relationships for impurity removal of $\sim 1\text{ min}^{-1}$ for manganese and $\sim 3\text{ min}^{-1}$ for iron at 90 °C in alkaline hypochlorite.

Received 10th February 2022,
Accepted 11th January 2023

DOI: 10.1039/d2ew00109h

rsc.li/es-water

Water impact

Reducing the amount of manganese and iron impurities present in drinking water treatment chemicals can improve both the aesthetic water quality and the integrity of its distribution pipelines, as it reduces the occurrence of discoloured water and pipescaling. Herein, we develop treatments to remove these species from lime hydrate manufactured for the water industry, and provide “rules-of-thumb” for their scale-up.

Introduction

Although access to safe drinking water is a mandated human right,¹ clean water distribution has been plagued by pipeline

integrity issues, even in high-income countries, for at least the last 90 years.² In England, drinking water, supplied by water companies and authorities, is subjected to economic, environmental and public health regulation, by the Water Services Regulation Authority (Ofwat), the Environment Agency, and the Drinking Water Inspectorate (DWI), respectively.³ Drinking water quality is governed by compliance with legislative standards (such as the European Drinking Water Directive 98/83/EC), which are based on guidelines published by the World Health Organisation.⁴ These standards set upper limits on the presence of a wide range of ions and compounds, predominantly based on their toxicity; potable water is frequently contaminated by both natural effects (associated with groundwater/reservoir hydrology and biology),⁵ and anthropogenic causes.⁶ These

^a Singleton Birch, Ltd., Melton Ross Quarries, Barnetby DN38 6AE, North Lincolnshire, UK. E-mail: dkocsis@singletonbirch.co.uk, chrismeyer747@gmail.com, j.wadhawan@hull.ac.uk

^b Department of Chemical Engineering, The University of Hull, Cottingham Road, Kingston-upon-Hull HU6 7RX, UK

^c Aura Innovation Centre, Bridgehead Business Park, Meadow Road, Hessle HU13 0GD, UK

^d Department of Chemistry, The University of Hull, Cottingham Road, Kingston-upon-Hull HU6 7RX, UK

† Electronic supplementary information (ESI) available. See DOI: <https://doi.org/10.1039/d2ew00109h>



impurities can be removed in water treatment works through the addition of chemical coagulants (such as alum and ferric sulphate) followed by clarification and filtration, with a subsequent disinfection step using, amongst others, chlorine or ozone, to remove micro-organisms.⁷ There is an additional consequence for drinking water treatment that results from the historical use of lead piping infrastructure in its distribution: the corrosion of this material is a public health hazard (most infamously demonstrated through the 2014–19 Flint water crisis);⁸ plumbosolvency control in the water mains relies on tiny solubility products, necessitating the addition of phosphates during water treatment, so as to maintain an extremely low concentration of soluble lead ions.

Manganese and iron are two essential mineral elements which are, likewise, regulated as a result of both toxicity (as Mn²⁺), and their propensity (as black and red oxides) to cause pipe-scale^{4,9} – the lining of the water distribution pipelines, causing restricted flow, and ultimately requiring more energy to be expended so as to deliver water to consumers than in a de-scaled pipeline. Although iron in drinking water is generally present at sufficiently low concentrations so as not to present a health hazard (there is no toxicity-based limit on iron in drinking water), manganese in drinking water may have adverse effects on intellectual and cognitive development, causing it to have an upper guideline value of 400 ppb.^{4,9} Nevertheless, the guidelines recommend upper thresholds on manganese (50 ppb) and iron (200 ppb), to reduce “metallic taste” and prevent so-called “black water” and “red water” phenomena, respectively.^{4,9} In the UK, these two discoloured water types are often a source of customer contacts (complaints) with water companies and authorities: in 2020, 1.8 M consumers (up from 1.1 M in 2019) were affected by the supply of tap water with an unaesthetic appearance (colour, taste and odour), as catalogued in the Chief Inspector's Report from the DWI,¹⁰ with the largest number of complaints stemming from North-West England, the Midlands and Wales – areas where the water supply is fed by upland surface waters.^{10,11} Such contacts cause the water companies and authorities to be fined by Ofwat. These problems with drinking water distribution arise from a variety of factors, such as the increase in water use due to hot weather,^{10,11} the inadequate treatment of raw waters,^{11,12} or during the improvement of the energy efficiency of water distribution by dislodging manganese- and iron-based oxide debris and pipe-scale using increased hydraulic pressure.^{9,11,12} Since the solubility of manganese and iron oxides is both redox- and pH-sensitive, control of manganese and iron in the water supply is achieved through (1) understanding reservoir geology and water hydrology,¹¹ (2) designing water treatment works to incorporate elaborate filtration operations,¹³ which may be gravel-based, or involve “greensand” (glauconite, (K, Na)(Fe^{III}, Al, Mg)₂(Si, Al)₄O₁₀(OH)₂, coated with manganese dioxide), and (3) reducing the amount of manganese-oxidising bacterial biofilms,^{9,12a,14} *via* efficient disinfection of the water supply.^{9,15,16}

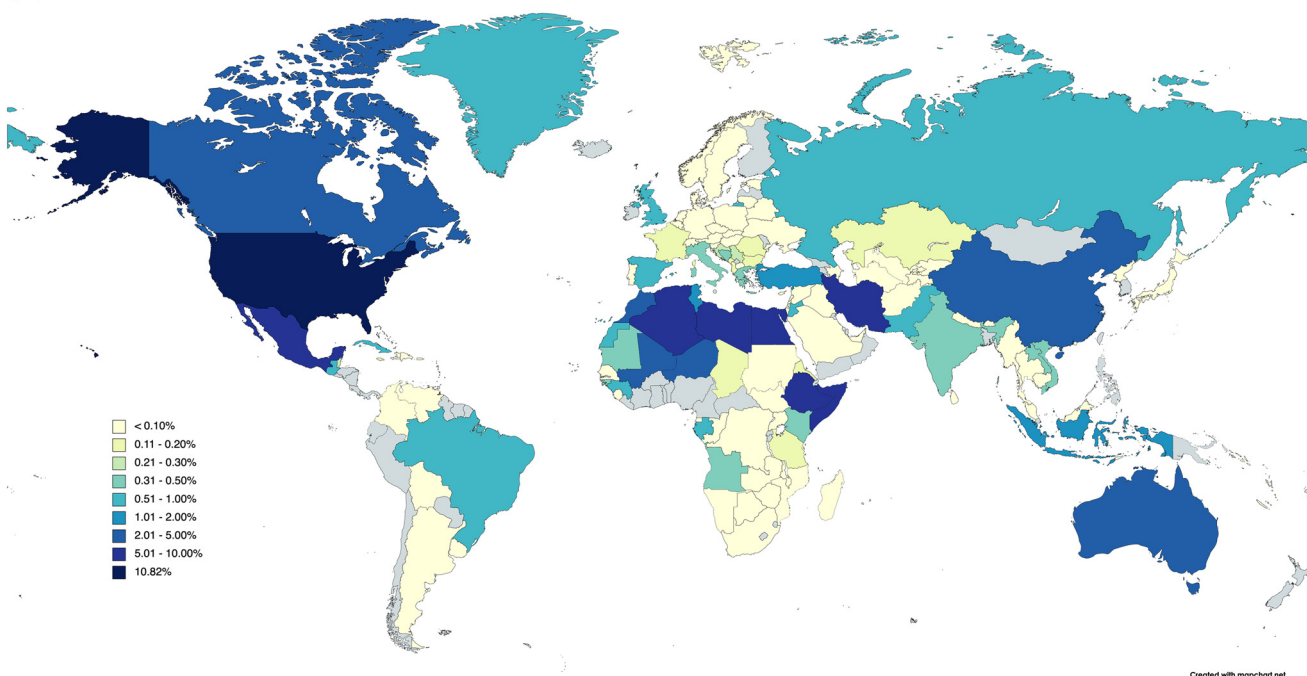
It is also important to control the impurity level present in the chemicals used to treat drinking water: the volume of chemicals used in water treatment means that even small reductions can provide benefit. Alkalies (pH modifiers) represent one of the largest group (by volume) of chemicals used by the UK water industry (in excess of 70 kTe y⁻¹),¹⁷ with a slight favouring (53%) of slaked lime (portlandite, lime hydrate, Ca(OH)₂) over caustic soda (NaOH).^{17a} Lime is unusual in that it can be used both to remove manganese from reservoir water,^{2,18a,b} and, as observed in KwaZulu-Natal, South Africa, brown lime (added during the treatment process) can be a source of manganese, even when the raw water has appreciable amounts of manganese.^{18c} Lime softening of water through impurity removal is thought to occur *via* carbonation of portlandite,^{19a} followed by heavy metal removal through sorption.^{19a,b} Removal of impurities containing silicon and phosphorous can be achieved through their reactive addition to lime or hydrate.^{19c} In the UK, water-grade alkalies currently conform to European Standard CEN TC 164/WG9/TG5, with purity criteria for both caustic (BS EN 896) and lime (BS EN 12518) regulating the concentrations of fluorides, radionuclides and heavy metals (arsenic, cadmium, chromium, mercury, nickel, lead, antimony and selenium), with further limits imposed on lime for SiO₂, Al₂O₃, Fe₂O₃, MnO₂ and CaCO₃ impurities.^{17a} This mandates the use of lime derived from industrial grade limestones only for water treatment. Such limestones are often referred to as pure carbonates (>95 wt% combined CaCO₃ and MgCO₃), which are readily available across the globe: Fig. 1a depicts the distribution of the total area (4.1 million km²) of pure carbonate outcrops in the world,²⁰ with the distribution of the manufacture of 420 MTe y⁻¹ of lime (the average global production rate in 2016–2020)^{21a} presented in Fig. 1b. Using the data for the UK as an example, we estimate that *ca.* 2 wt% of all lime production is required for water treatment purposes,^{21b} so that the global requirement of lime hydrate is *ca.* 11 MTe y⁻¹ – a quantity that is not economically viable to manufacture without calcination of limestone.

The British Geological Survey have mapped the areas where pure calcium carbonate outcrops occur in England and Wales (see Table 1);²² current UK lime manufacturing²³ uses either the high- or very high- purity limestones found in North Lincolnshire (Welton formation of Cretaceous chalk)²⁴ or the Derbyshire Dome (Bee Woo formation of Carboniferous limestones).²⁵ However, although these are all >97 wt% CaCO₃, they are typically not “manganese-free”, and therefore may introduce manganese into the drinking water distribution network, unless first cleaned to remove the manganese impurities.

In this paper, we illustrate redox chemical processes to treat water-grade lime derived from both high-purity and very high-purity limestones, so as to reduce the extent of manganese and iron impurities that they contain. We use insights into the physicochemical dynamics underpinning the impurity removal process to develop important design



(a)



(b)

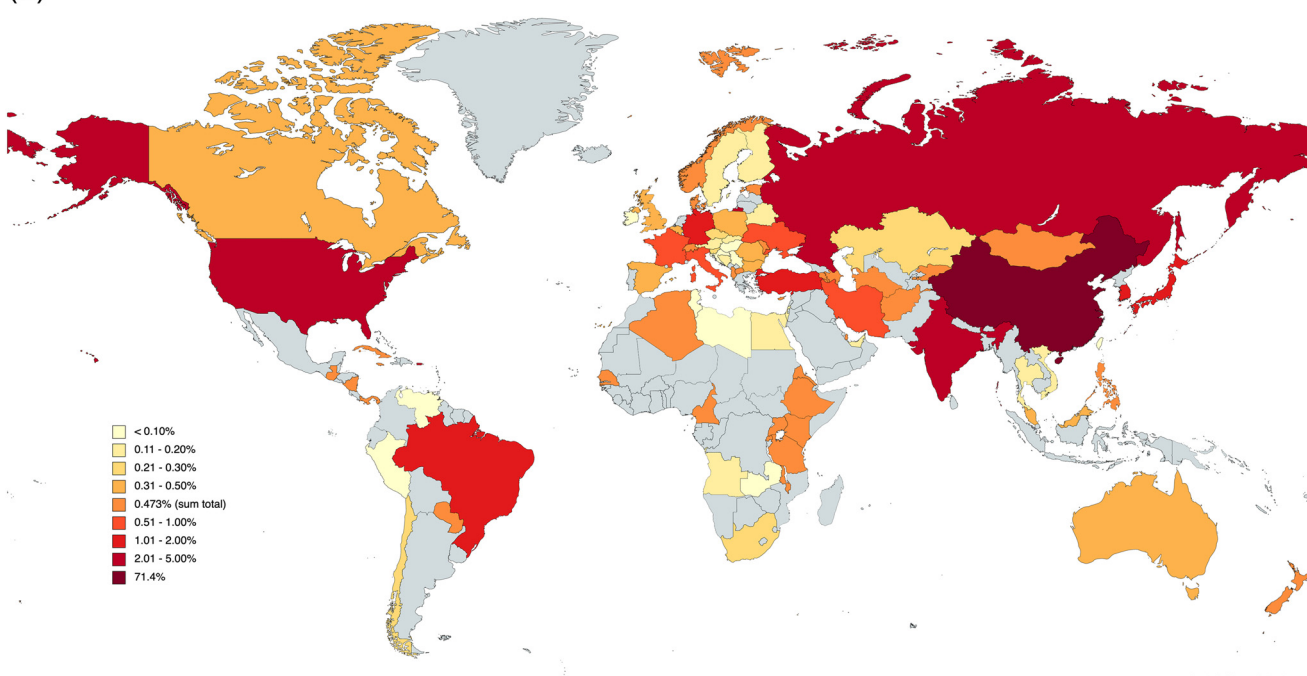


Fig. 1 World distribution maps illustrating the country breakdown of (a) pure carbonate rock outcrops, and (b) lime production. In both cases, data are expressed as a percentage of the world totals: (a) 4.1 million km² and (b) 420 MTe y⁻¹ (average for 2016–2022), with the country with the greatest pure carbonate rock outcrop area (USA) or the highest lime production (Republic of China) indicated separately. Note that in (b), only the sum total of the individual countries is given with the colour corresponding to 0.473%, and that other nations (in grey) may have produced lime over the 2016–2020 period. Data taken from (a) ref. 20, and (b) ref. 21, with both maps being drawn using software available at MapChart.Net.

relationships for suitable process operations that could be integrated within existing lime manufacturing plants. We first provide an overview of the distribution of these

impurities in both Carboniferous limestone and Cretaceous chalk (see ESI†), and indicate how these change during the lime cycle for the production of slaked lime.



Table 1 Typical iron and manganese impurity levels in industrial grade limestones in England and Wales^{a,b}

Location	Formation	CaO/wt%	Fe ₂ O ₃ /wt%	MnO/wt%
<i>Carboniferous limestone</i>				
Peak District	Bee low	55.41	0.07	0.02
Mendips	Burrington oolite	55.24	0.01	0.00
South Wales	Oxwich head	55.80	0.02	0.01
North Wales	Llandulas	55.38	0.10	0.15
North Pennines	Cove	55.73	0.01	0.01
Lake District	Park	55.52	0.03	0.05
<i>Average (Carboniferous limestone)</i>		55.51	0.04	0.04
<i>Standard deviation</i>		0.21	0.04	0.06
<i>Cretaceous chalk</i>				
Humberside	Welton	54.81	0.04	0.05
Humberside	Flamborough	53.60	0.10	0.06
Wiltshire	Upper chalk	54.87	0.06	0.15
Wiltshire	Upper chalk	54.93	0.03	0.03
Kent	Upper chalk	55.45	0.04	0.04
Suffolk	Upper chalk	54.94	0.08	0.06
<i>Average (Cretaceous chalk)</i>		54.77	0.06	0.07
<i>Standard deviation</i>		0.62	0.03	0.04

^a Adapted from data provided as Tables 3 and 12 in ref. 22c. ^b Very high purity limestone is >98.5 wt% CaCO₃, corresponding to >55.2 wt% CaO; high purity limestone has CaCO₃ in the range 97–98.5 wt%, corresponding to CaO in the range 54.3–55.2 wt%, using conventional assessment criteria – see Table 5 of ref. 26a. Note that the Flamborough chalk formation is technically of medium purity.

Manganese and iron impurities in high purity limestones

The British Geological Survey describes limestones as being high purity, or very high purity depending on whether the mass fraction of CaCO₃ present therein is between 97.0% and 98.5%, or above 98.5%, respectively.²⁶ These are the only two categories of limestone considered to be suitable as industrial grade for use in the water treatment, iron and steel, chemicals, glass making, filters and pigments, paper and flue gas desulphurization industries.^{22,27} Table 1 illustrates the typical compositional variation of both manganese (as MnO) and iron (as Fe₂O₃) impurities within high and very high-purity limestone (limestone and chalk) strata in England and Wales.^{22c} It is clear that, with the exception of the Burlington oolite, all high-purity (Cretaceous) and very high-purity (Carboniferous) limestones in Table 1 are contaminated by both iron and manganese, with the slightly lower purity chalk being more uniform in its impurity distribution – the relative standard deviations are high for Carboniferous limestones (92% (Fe) and 141% (Mn)), but much lower for the Cretaceous chalk (47% (Fe) and 67% (Mn)), across all locations. This general picture is slightly misleading, since different parts of a limestone quarry can expose different depths of the limestone stratigraphy – for example, the Hindlow Quarry (Carboniferous limestone from the Peak District) is reported to have manganese levels between 80–160 ppm, and iron levels between 200–500 ppm;²⁵ in contrast the Tunstead Quarry (Carboniferous limestone from the Peak District) has manganese levels in the range 80–960 ppm, with iron levels ranging between 200–3000 ppm.²⁵ It appears that small variations in the rock lithology can lead to a wide variation

in the level of the iron and manganese contaminants;^{22,26} such local variations can downgrade the purity of limestones,^{22,26} and, since limestones (including hard Northern Province chalk – see ESI†) are typically blasted from a rock face, it is not always possible to separate out these impurities.²⁷

Manganese and iron impurities in limestones derive from a number of sources, such as the iron sulphides (pyrite and marcasite) present in clay bands (wayboards), through dolomitization (minerals such as ankerite and kutnohorite), or through “accessory” minerals including tourmaline, garnet, magnetite, rhodochrosite and siderite.^{22,24,25,28} Since limestones are permeable, it is thought that incongruent reactions at the particle surfaces release Mn²⁺ and Fe²⁺ ions into either recharge or connate water, resulting in a purer calcite.²⁸ Thus, under oxidising conditions ($E_h > ca. 300$ mV, see ESI†), manganese and iron can be deposited as dendrites at shallow fracture surfaces as the oxides (such as pyrolusite, MnO₂), sesquioxides (braunite, Mn₂O₃, bixbyite, and haematite, Fe₂O₃), oxohydroxides (for example, manganite, MnOOH, and goethite, α -FeOOH), hydroxides and hydrated iron oxides (including limonite).^{29–32} Typically iron and manganese oxides in limestones occur in separate deposits. However, where they occur together, the iron oxides typically overlay the older manganese oxide deposits,²⁹ indicating that the manganese oxides enable the precipitation of iron oxides.³³ Under reducing conditions, the divalent impurities can be incorporated as interstitial solid solutions in the calcite (or, in the case of Limestone, calcite and aragonite) particles.^{29,34} Such solution/re-deposition chemical processes (see Fig. 2) are characteristic origins of manganese ores,²⁹ including the famous deposits at Nikopol (Ukraine) and Chiaturi (in the Caucasus).³⁵



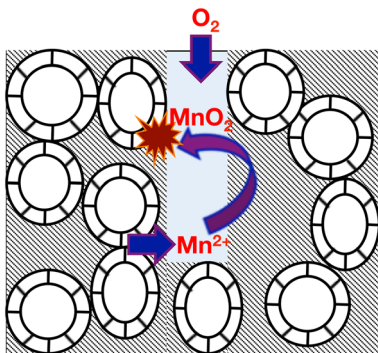


Fig. 2 Schematic illustration of dissolution/re-precipitation reactions causing the mineralisation of manganese (as radial dendritic growths) through incongruent reactions at fracture surfaces in the presence of interstitial or connate or recharge water. Adapted from ref. 28.

Manganese and iron impurities in slaked limes

The manufacture of lime hydrate first involves the comminution of limestones, followed by the stages of calcination and then reaction with water (see ESI†).²⁷ During the calcination process to form quicklime (CaO , molar mass 56 g mol^{-1}), carbon dioxide is lost from the calcite (CaCO_3 , molar mass 100 g mol^{-1}), so that although there is a small degree of shrinkage of the rock,²⁷ the concentration of solid impurities increases. Singleton Birch Ltd.'s high-calcium quicklime, Burnt Lime 40,³⁶ although hard to quantify exactly owing to its high reactivity with atmospheric moisture and carbon dioxide, typically comprises >90 wt% CaO , with small degrees of impurities derived from both the limestone rock and the sulphur from the natural gas used in the calcination. Digestive analysis (see ESI†) of quicklime indicates a doubling of the manganese and iron concentration in lime compared with chalk (Fig. 3). No differences were found between the size fractions investigated ($\sim 50 \text{ mm}$ for Burnt Lime 40, or

3.35 mm finer screenings). The slight difference between the ratios for manganese and iron in lime *versus* the quarried rock, is indicative of the fact that both impurities derive from different oxidation forms in the chalk: the mass loss is consistent with Fe_2O_3 (Fe^{III}) and Mn_3O_4 (hausmannite, where Jahn–Teller distorted Mn^{III} occupies all of the octahedral sites, with Mn^{II} distributed in the tetrahedral sites in a cubic oxide lattice) being the impurities in quicklime, and Mn_2O_3 and either FeCO_3 or FeS_2 as the impurities in the chalk. This interpretation is consistent with the reported thermodynamic stability of manganese and iron oxides, carbonates and disulphides at kiln temperatures ($900\text{--}1100 \text{ }^{\circ}\text{C}$).^{37,38} Note that whilst the kiln temperature is controlled to avoid sintering (dead-burned lime), the maximum upper temperature is close to that for the tetragonal-to-cubic phase change of the hausmannite spinel ($1170 \text{ }^{\circ}\text{C}$).³⁹

Slaked lime is manufactured through reacting quicklime with a slight excess of the stoichiometric amount of water, to afford lime hydrate ($\text{Ca}(\text{OH})_2$). The exothermicity of this reaction (temperatures can reach up to $150 \text{ }^{\circ}\text{C}$) causes the excess water to vaporise, so that the impurities will remain in the solid state. The lime hydrate is a fine white powder, with an average particle diameter of $5 \text{ }\mu\text{m}$, and is a porous material of extremely high specific surface area ($>20 \text{ m}^2 \text{ g}^{-1}$).³⁶ As indicated in Fig. 3, on slaking the lime, the mass increase in going from CaO to $\text{Ca}(\text{OH})_2$ (molar mass 74 g mol^{-1}) causes the impurity concentration to decrease by similar amounts for manganese and iron impurities. This suggests that the chemical nature of the manganese impurity is essentially unaffected by slaking, even if the iron contaminants form hydrated oxides. As indicated in ESI† slaked lime manufactured by Singleton Birch Ltd. is typically *ca.* 97 wt% portlandite ($\text{Ca}(\text{OH})_2$). Accordingly, we may envisage that the particles of lime hydrate can be considered as existing with both “hard” core of CaCO_3 surrounded by a “softer”, porous shell of $\text{Ca}(\text{OH})_2$. This visualisation is a little primitive, since re-carbonation of the surface of the intermediate lime particles can take place. Nevertheless, in terms of impurity distribution and dispersion, we consider the following: Fe_2O_3 (core/shell), $\text{FeS}_2/\text{FeCO}_3$, (core), Mn_2O_3 (core) and Mn_3O_4 (core/shell).

The manganese and iron impurities in lime hydrate cannot be removed by water alone, as will be discussed later. It follows that a solution-based chemical etching process is necessary to remove iron and manganese impurities from lime hydrate. However, as the hydrate buffers the solution at very high pH (*ca.* 12.3), an etching process involving reduction of the impurities to the soluble divalent ions is flawed, as this will cause the impurities to be precipitated as the (coloured) hydroxides onto the white hydrate.⁴⁰ Accordingly, we consider the oxidative etching of the impurities.

Oxidative removal of manganese and iron impurities from slaked lime

In preliminary experiments, 1 g of slaked lime were incubated overnight with 100 g (80 mL) of alkaline hypochlorite solution ($\sim 8\%$, density $\sim 1.25 \text{ g mL}^{-1}$) and left,

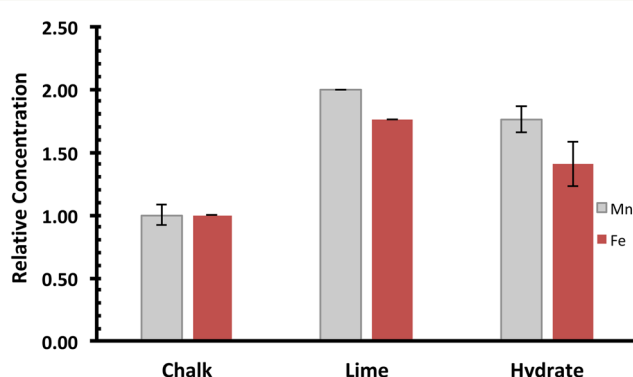


Fig. 3 Manganese and iron impurities within the lime cycle (chalk is CaCO_3 ; lime refers to CaO ; hydrate refers to $\text{Ca}(\text{OH})_2$). Data obtained through HF digestion of the sample, followed by ICP-OES analysis (see ESI†). Note that in these plots, manganese (grey) and iron (red) levels, recorded as ppm (mg kg^{-1}), have been normalised to the average manganese or iron level present in quarried chalk. Error bars indicate one standard deviation over at least three samples.



without stirring, in an open beaker at ambient temperature, after which a pale pink supernatant was observed. Spectroscopic analysis (see ESI†) afforded both a split-peak at *ca.* 520 nm, corresponding to the permanganate (MnO_4^-) anion, and a peak at 505 nm, which matches-up with that expected from ferrate (FeO_4^{2-}).⁴¹ Indeed, when the inverse spinel magnetite, Fe_3O_4 , was treated under similar conditions, a purple supernatant, corresponding to ferrate was observed. These experiments were repeated using slaked lime manufactured from rocks derived from throughout the Welton formation of the Cretaceous chalk at the Melton Ross Quarry (North Lincolnshire, UK), in addition to slaked lime derived from Bee low Carboniferous limestone (Derbyshire, UK), both in the presence and absence of oxygen. In these experiments, after soaking the slaked lime in alkaline hypochlorite for a variable, fixed time periods, the pink supernatant was removed through vacuum filtration, and owing to the reduction of the supernatant by the filter paper (see ESI†),⁴² only the upper part of the dried filter cake was analysed *via* ICP-OES. Fig. 4 illustrates the temporal variation

of both the manganese and the iron in the filter cake, where it is clear that after *ca.* 72 h of incubation, the manganese level drops by *ca.* 60%, and the iron content decreases by *ca.* 70%. These results are general, and hold irrespective of the origin of the slaked lime feedstock – Northern Province Cretaceous chalk (derived from a wide range of lithostratigraphies within the Welton formation) or Carboniferous limestone (Bee low formation). However, there is a subtle difference in the trends for manganese and iron: the filter cake becomes progressively depleted from manganese impurities during the treatment (irrespective of whether oxygen is present), at an initial rate of $\sim 1\% h^{-1}$; in contrast, the removal of iron impurities is affected by the presence of oxygen in the solution. Under aerobic conditions, the iron content of the filter cake appears first to increase, and then decrease; however, there is no apparent loss of iron impurity under anaerobic conditions.

These results indicate that the removal of both the manganese and the iron impurities occurs in slightly different ways, likely linked to the difference in the oxidation

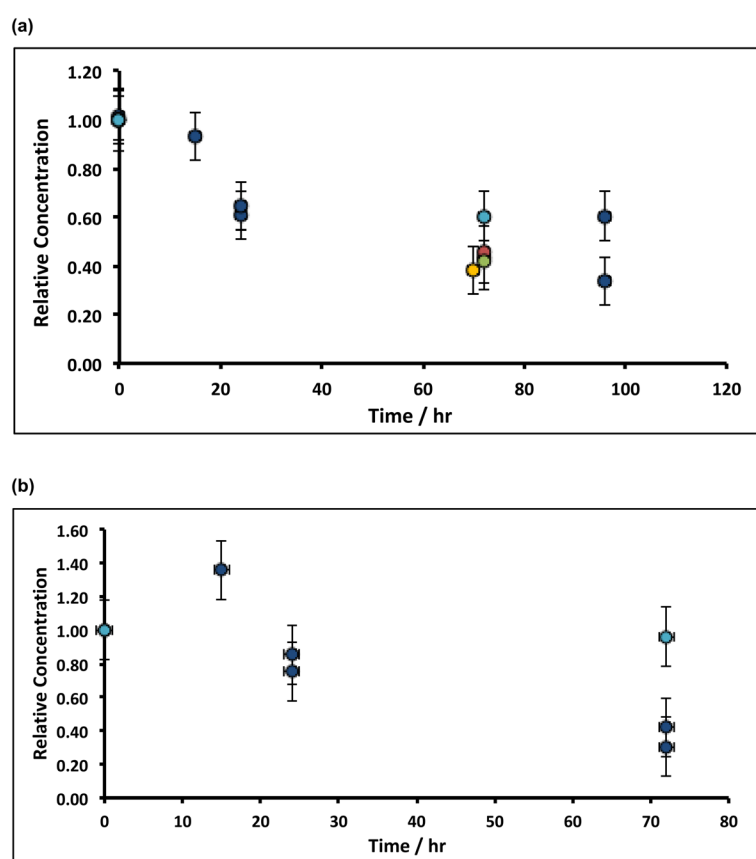
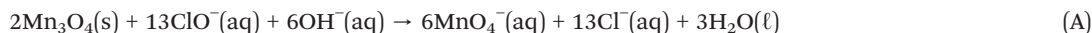


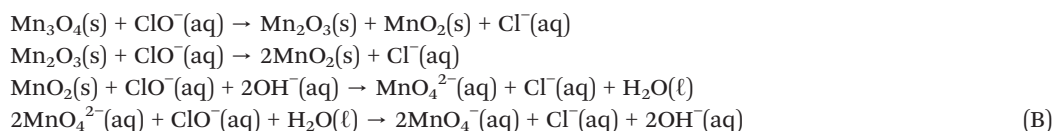
Fig. 4 Variation of (a) Mn and (b) Fe under quiescent conditions during incubation with 8% alkaline hypochlorite solution. Note that the data have been normalised to the average manganese or iron level present in untreated sample (when time = 0 h, and where the relative concentration is unity). Unless stated, experiments were undertaken without oxygen purged-solutions. Key: Dark blue circles correspond to lime hydrate derived from Welton formation chalk derived from screenings obtained from the middle stratigraphic section (between the Melton Ross Marl and the Barton Marl 1); red circles correspond to slaked lime derived from Bee Woo limestone; green and gold circles correspond to lime hydrate derived from chalk or chalk screenings, respectively, taken from the bottom bed (between the Grasby Marl to just below the Chalk Hill Marl, but above the black band); light blue circles correspond to conditions identical to the dark blue circles, except under anaerobic (oxygen-purged) conditions. Error bars indicate one standard deviation over at least three samples.



states of the two different transition metal ion impurities, and reaction mechanism. The manganese is present in Mn_3O_4 as both Mn^{II} and Mn^{III} , so that oxidation to Mn^{VII} can be achieved through reaction with alkaline hypochlorite, without requiring the presence of oxygen.



This reaction (A) does not have to occur in a single step; rather, since the presence of green Mn^{VI} is noticeable during the filter paper reduction of the supernatant (see ESI†), we may propose the following reaction sequence.



This scheme is in agreement with literature observations on the oxidation of manganese species at high pH to afford permanganate.⁴³ Indeed, we observed that pyrolusite ($\beta\text{-MnO}_2$) behaved in an analogous manner (data not shown). Note that, in agreement with literature observations for aragonite,⁴⁴ we were unable to observe the removal of manganese from chalk immersed in alkaline hypochlorite.

In contrast, since the iron impurities are present as Fe^{III} , the oxidation to afford Fe^{VI} in the presence of concentrated sodium hydroxide (which stabilises the hypochlorite solution) must occur first through the solubilisation of the Fe^{III} species,⁴⁵

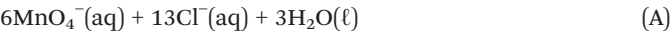


In the above, although we have depicted the iron impurities as haematite ($\alpha\text{-Fe}_2\text{O}_3$), we recognise this could be a different form of Fe^{III} . This solubilisation is also observed as a route for removing iron impurities from aragonite.⁴⁴ Indeed, we also observed that maghaemite ($\gamma\text{-Fe}_2\text{O}_3$) was partially solubilised by oxygenated, concentrated sodium hydroxide solution when incubated overnight, affording a pale yellow solution, corresponding to ferrite (data not shown). This is consistent with the low solubility of ferric oxide at ambient temperature,⁴⁵ which is reported to increase with both temperature and hydroxide concentration; it has been recognised that the solubility of haematite in alkali-metal hydroxide solutions changes with the alkali metal cation, and



follows the order for oxygen oxidation of metallic iron in those solutions.^{45b}

In the absence of oxygen, there is little loss of iron from the filter-cake (Fig. 5) in the presence of alkaline hypochlorite, suggesting no oxidation takes place. However, in the presence of oxygen, the concentration of iron in the filter-cake first increases (by 40%), and then reduces to close



However, half-reaction (D) is viable for alkaline hypochlorite: the standard potential for the ferrite/ferrate redox couple, though not very well defined,^{43c,45a} is estimated to be $\sim +0.8\text{--}0.9\text{ V vs. SHE}$ at pH 14. We thus propose that in the absence of oxygen, Fe_2O_3 (or some hydroxylated solid form) remains in the solid state; in the presence of oxygen, adsorption onto the surface of the iron(III) oxide/oxohydroxide first enables solid $\text{NaFeO}_2(\text{s})$ to form (giving rise to the 40% increase in concentration),^{45b,c} which can then dissolve under oxidative conditions to yield the purple ferrate ion in solution. To confirm this, an experiment was undertaken in which magnetite (Fe_3O_4 – an inverse spinel with Fe^{III} in the tetrahedral sites and half of the octahedral sites, with the remaining octahedral sites occupied by Fe^{II}) was incubated with oxygenated, concentrated sodium hydroxide solution. After one week of incubation, the supernatant above the black solid was still clear and colourless; addition of alkaline hypochlorite caused no immediate colour change, except after an overnight incubation, whence the deep purple ferrate anion was observed.

In contrast, experiments using an ironstone ($\sim 82\%$ calcite, $\sim 17\%$ goethite and $<1\%$ siderite, see ESI†) under reflux at $90\text{ }^\circ\text{C}$ with alkaline hypochlorite did not give rise to a purple solution, indicating the need for ferrite formation to occur through dissolution prior to oxidation.

This confirms the nature of the oxidative etching process of iron-based impurities in lime, which can be written as the overall reaction:

Although no effort was made to shield the solutions from direct sunlight, it is unlikely that photo-reductive dissolution

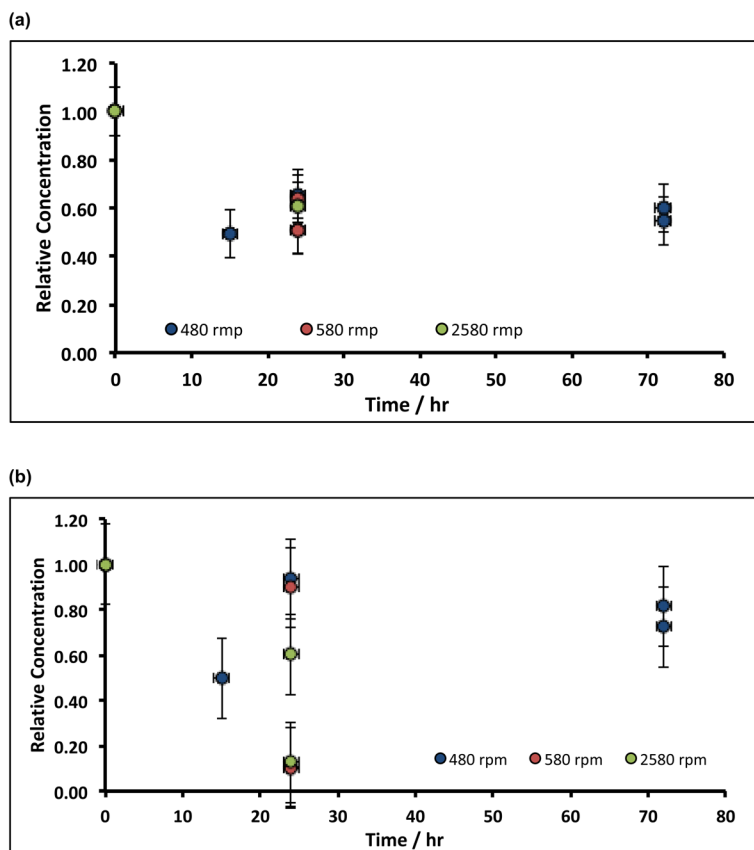


Fig. 5 Variation of (a) Mn and (b) Fe under stirred conditions (indicated by the rotation speed of the magnetic flea used) during incubation with 8% alkaline hypochlorite solution. Note that the data have been normalised to the average manganese or iron level present in untreated (and unstirred) sample (when time = 0 h, and where the relative concentration is unity). All experiments were undertaken under aerobic conditions with lime hydrate derived from Welton formation chalk derived from screenings obtained from the middle stratigraphic section (between the Melton Ross Marl and the Barton Marl 1). Key: dark blue circles correspond to rotation speeds of 480 rpm; red circles correspond to rotation speeds of 580 rpm; green circles correspond to rotation speeds of 2580 rpm. Error bars indicate one standard deviation over at least three samples.

of Fe^{II} by superoxide⁴⁶ is viable in these experiments: superoxide is readily oxidised by hypochlorite.

From a chemical process perspective, it is insightful to identify whether the chemical etching process is limited by slow transport of hypochlorite to the slaked lime particle surface, or by slow surface kinetics: in the former case, greater impurity removal will occur with increased agitation of the slaked lime/alkaline hypochlorite slurry; in the latter, greater removal necessitates longer incubation times. The comparison of Fig. 5 with Fig. 4 indicates that increasing the agitation of the hydrate/hypochlorite solution slurry does not translate into a greater loss of manganese from the resulting filter cake, implying that the etching is limited by the surface kinetics; this is less evident for the case of iron removal, as expected from the inferred solubilisation prior to oxidation (reaction (E)).

Owing to the control due to slow surface kinetics (*ca.* 50% of impurity removal through chemical etching using alkaline hypochlorite requires between 10–20 h), reaction variables (such as temperature and hypochlorite concentration) were next varied, so as both to unravel the mechanism further, and to optimise the impurity-removal chemistry, in order to develop a more useful and practical process operation.

Optimisation of dissolution process chemistry

Under aerobic conditions, increasing the temperature from ambient (20 °C) to 90 °C in ~8% alkaline hypochlorite solution, causes the initial rate of removal of both manganese and iron impurities in the filter cake to increase to *ca.* 1% min^{-1} (Mn) and *ca.* 3% min^{-1} (Fe), Fig. 6. This increase does not result from an apparent increase in solubility: the retrograde solubility of $\text{Ca}(\text{OH})_2$ with temperature,⁴⁷ in addition to the common-ion effect, serves to reduce hydrate dissolution to negligible values (~0.003 wt%, see ESI†). Indeed, control experiments using deionised water (1.0 g of lime hydrate equilibrated (20 min at 90 °C) in 80 mL of deionised water), reveal a 20% increase in the concentration of manganese in the solids, but *ca.* 60% decrease in iron (Fig. 6). Inasmuch as an increase in the manganese content is expected: ~5 wt% of hydrate will dissolve (see ESI†), enriching the impurity concentration, the decrease in iron content of the resulting filter cake is consistent with the formation (and thermally enhanced solubility) of ferrite.^{45b} Again, the effect of increasing the



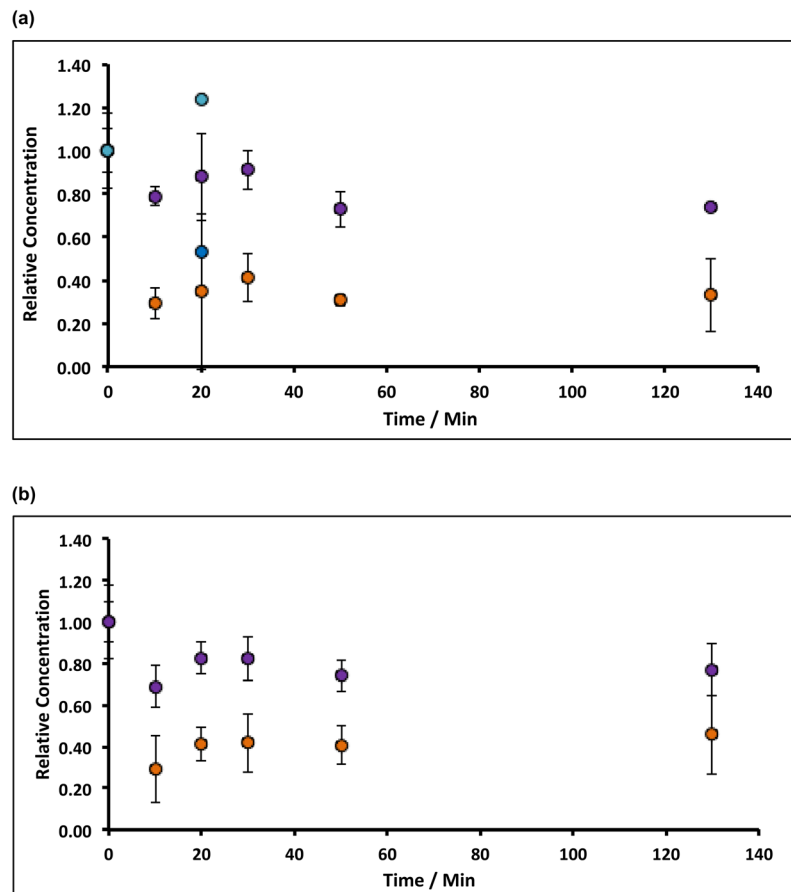
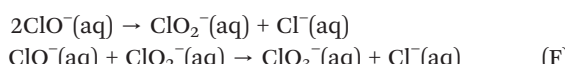


Fig. 6 Variation of Mn and Fe concentrations in lime hydrate filter cake during incubation with 8% alkaline hypochlorite solution or deionised water at 90 °C, under (a) non-stirred but thermally convective, and (b) stirred at an arbitrary rotation speed of the magnetic flea used. Note that the data have been normalised to the average manganese or iron level present in untreated (and unstirred) sample (when time = 0 h, and where the relative concentration is unity). All experiments were undertaken under aerobic conditions with lime hydrate derived from Welton formation chalk derived from screenings obtained from the middle stratigraphic section (between the Melton Ross Marl and the Barton Marl 1). Key: purple circles correspond to Mn concentrations using alkaline hypochlorite solution; sky blue circles correspond to Mn concentration using deionised water; orange circles correspond to Fe concentrations using alkaline hypochlorite solution; blue circles correspond to Fe concentration using deionised water. Error bars indicate one standard deviation over at least three samples.

mass transport of hypochlorite (higher than that due to thermal convection) has only very limited effect (Fig. 6).

The plots in Fig. 6 indicate that prolonged incubation at 90 °C has little effect on the etching. This likely results from the thermal decomposition of hypochlorite, which can be catalysed by ferric oxide, and is thought⁴⁸ to proceed *via* a slow initial disproportionation reaction of hypochlorite to chlorite, followed by faster oxidation to chlorate:



It follows that a cascade chemical etching process, where in a batch of slaked lime is treated for a fixed, short period of time (intervals of 1, 2 and 3 h) at 90 °C with alkaline hypochlorite, filtered and then re-treated using fresh hypochlorite reagent under the same conditions, would enable shorter treatment times and, overall faster impurity removal. This is indeed observed, as illustrated in Fig. 7 and 8, where it is appreciated that the initial rate of removal with

fresh hypochlorite solution is maintained though this staged process. Moreover, as expected, the shortest cascade incubation (20 min) soonest yields the purest filter cake (Fig. 8) in terms of manganese and iron removal. Again, the contrast between the iron and the manganese data is likely due to the requirement to solubilise the iron species as ferrite, especially at the higher temperature, suggesting that this first step (assisted by oxygen) is rate-determining for iron impurity removal at the higher temperature.

Under these conditions of temperature (90 °C) and cascade interval (20 min), increasing the hypochlorite concentration from ~8% to ~14% (a concentration factor of 1.75), has little effect on the removal of manganese or iron (Fig. 8). This indicates that removal of both manganese and iron follows zeroth-order kinetics in hypochlorite in both cases. Focussing on the mechanistically less complicated manganese dissolution, the manganese-removal rate,

$$\frac{d(n_{\text{Mn}})}{dt} = -k_{\text{het}} \quad (1)$$



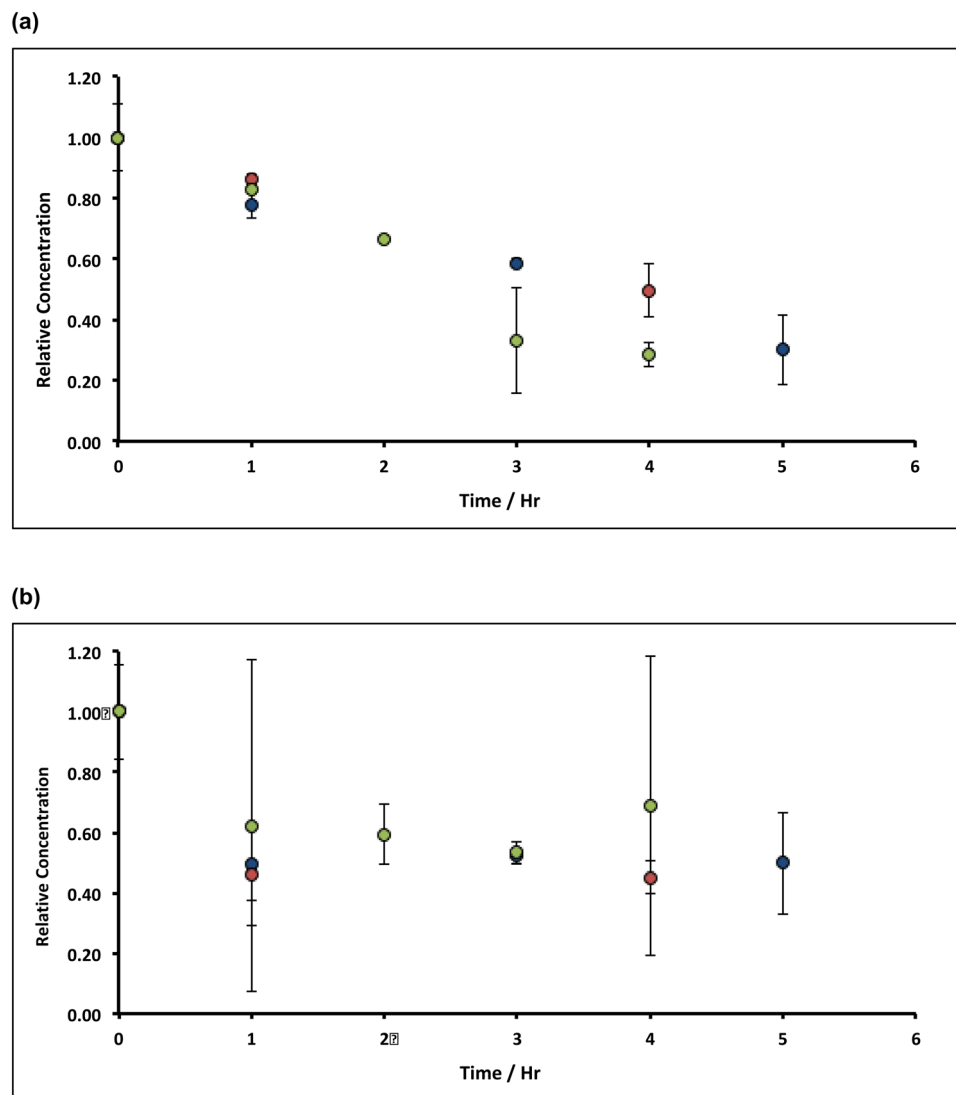


Fig. 7 Variation of (a) Mn and (b) Fe concentrations in lime hydrate filter cake during variable time incubation intervals (1, 2 and 3 h) with 8% alkaline hypochlorite solution or deionised water at 90 °C whilst stirred at an arbitrary rotation speed of the magnetic flea used. Note that the data have been normalised to the average manganese or iron level present in untreated (and unstirred) sample (when time = 0 h, and where the relative concentration is unity). All experiments were undertaken under aerobic conditions with lime hydrate derived from Welton formation chalk derived from screenings obtained from the middle stratigraphic section (between the Melton Ross Marl and the Barton Marl 1). Key: green, blue and red circles correspond to incubation times of 1, 2 and 3 h, respectively. Error bars indicate one standard deviation over at least three samples.

where $(n_{\text{Mn}})_{\text{solid}}$ is the number of moles of manganese in the solid lime hydrate (virgin material or filter-cake) to which alkaline hypochlorite solution is added, and k_{het} is the zeroth-order rate constant corresponding to the rate-limiting step in the sequence of steps provided in reaction (B) – see also ESI.† The solid manganese concentration determined using ICP-OES (see ESI†) affords manganese concentrations as parts-per-million by mass (ppm, mg kg⁻¹), so that at any time t , $(n_{\text{Mn}})_{\text{solid}}^t = \frac{10^{-6}(\text{ppm})^t \{m_s - qsV\}}{M_{\text{Mn}}}$, in which $(\text{ppm})^t$ is the manganese concentration in the filter-cake, m_s is the mass of the virgin lime hydrate used at the start of the experimental cascade (in g), s is the solubility of the lime hydrate in the alkaline solution at the experimental temperature (in g L⁻¹), V is volume of the alkaline hypochlorite solution used (in L),

which is kept at a constant value throughout the cascade, q is the cascade number, with the first batch taking $q = 1$, and M_{Mn} is the molar mass of manganese (in g mol⁻¹). This enables eqn (1) to be re-cast in terms of the solid manganese concentration, and integrated using the boundary condition $t = 0$, $(\text{ppm})^t = (\text{ppm})^0$, to yield eqn (2):

$$\frac{(\text{ppm})^t}{(\text{ppm})^0} = 1 - k_{\text{eff}}t \quad (2)$$

in which the effective rate constant, $k_{\text{eff}} = k_{\text{het}} \frac{10^6 M_{\text{Mn}}}{(\text{ppm})^0 \{m_s - qsV\}}$. For the extremely low lime hydrate solubilities (for further discussion, see ESI†), the corrected mass is essentially constant, so that plots of relative manganese concentration against time are linear, as

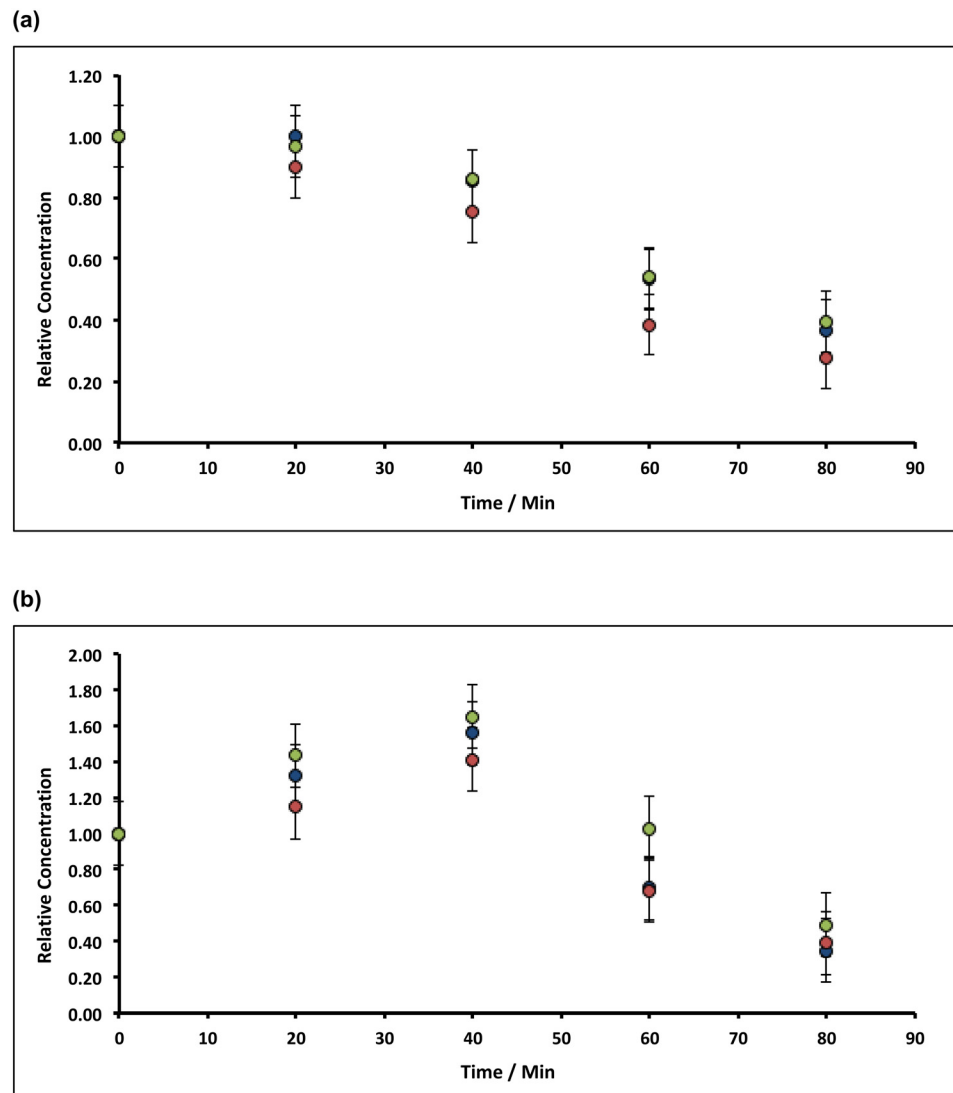


Fig. 8 Variation of (a) Mn and (b) Fe concentrations in lime hydrate filter cake during fixed 20 min incubation cascades with 8% or 14% alkaline hypochlorite solution or deionised water at 90 °C whilst stirred at an arbitrary rotation speed of the magnetic flea used. Note that the data have been normalised to the average manganese or iron level present in untreated (and unstirred) sample (when time = 0 h, and where the relative concentration is unity). All experiments were undertaken under aerobic conditions with lime hydrate derived from Welton formation chalk derived from screenings obtained from the middle stratigraphic section (between the Melton Ross Marl and the Barton Marl 1). Key: blue, red and green circles correspond to hypochlorite chloride levels of 8% (batch 1), 8% (batch 2) and 14%, respectively. Error bars indicate one standard deviation over at least three samples.

observed in Fig. 9 for small cascade numbers. These afford values of $k_{\text{het}} = 6.1 \pm 1.5 \times 10^{-8} \text{ mol min}^{-1}$ at 90 °C for the removal of manganese impurities in lime hydrate, which are independent of both the derived limestone type (Cretaceous chalk or Carboniferous limestone), and the mass of the material treated, suggesting all samples are approximately monodisperse and with similar particle sizes.

For manganese removal, these are pure kinetics – they have no contribution from mass transfer: under the approximation that the Sherwood number (Sh) is 2, *viz.*,⁴⁹ $\text{Sh} = \frac{d_p k_L}{D} = 2$, an equation relevant for mass transfer to small particles, where d_p is the slaked lime particle diameter (5 µm),³⁶ D is the diffusion coefficient of hypochlorite in aqueous alkaline solution ($\sim 10^{-5} \text{ cm}^2 \text{ s}^{-1}$), the mass transfer coefficient (k_L) is estimated as being 0.04 cm s^{-1} . In the experiments in Fig. 9, the etching

rate constant at 90 °C is $\sim 10^{-9} \text{ mol s}^{-1}$ from a surface area of³⁶ $\sim 20 \text{ m}^2 \text{ g}^{-1}$ using an hypochlorite concentration of $\sim 5 \text{ M}$, affording a mass transfer coefficient of $\sim 10^{-12} \text{ cm s}^{-1}$, which is many orders of magnitude less than the transport-limited rate, confirming no contribution from mass transfer.⁵⁰

The low temperature data illustrated in Fig. 4 can also be analysed through eqn (2), to afford $k_{\text{het}} = 8.0 \pm 3.4 \times 10^{-10} \text{ mol min}^{-1}$ at 20 °C for manganese removal from lime hydrate. Again, this is independent of the derived limestone type, and whether the etching is undertaken in the presence, or absence of oxygen. These low and high temperature rate constants enable the estimation of the activation barrier for the etching process to be $0.58 \pm 0.07 \text{ eV}$, using an Arrhenius-type relationship. This activation energy is similar to literature estimates for the DC conductivity (*via* electron hopping



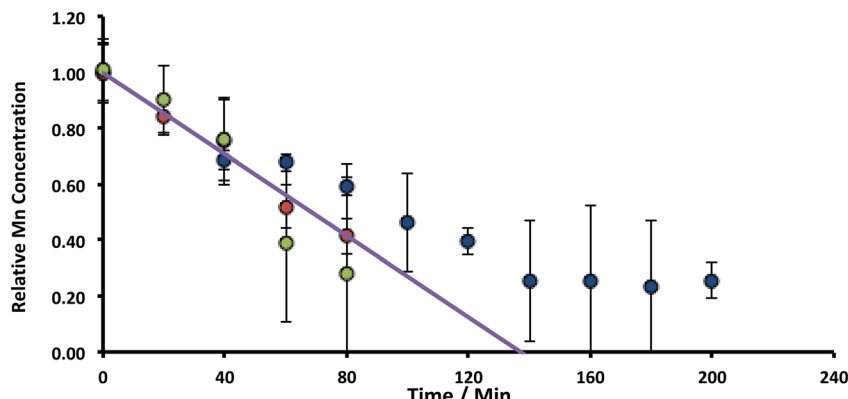
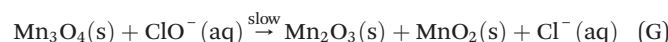


Fig. 9 Variation of Mn concentrations in lime hydrate filter cake during fixed 20 min incubation cascades with 14% alkaline hypochlorite solution or deionised water at 90 °C whilst stirred at an arbitrary rotation speed of the magnetic flea used. Note that the data have been normalised to the average manganese or iron level present in untreated (and unstirred) sample (when time = 0 h, and where the relative concentration is unity). All experiments were undertaken under aerobic conditions. Blue and green circles correspond to lime hydrate derived from Welton formation chalk derived from screenings obtained from the middle stratigraphic section (between the Melton Ross Marl and the Barton Marl 1), with initial hydrate mass of 2.0 and 1.0 g, respectively; red circles correspond to lime hydrate derived from Carboniferous limestone, with initial hydrate mass of 1.0 g. Error bars indicate one standard deviation over at least three samples. The purple line corresponds to eqn (2), with the average effective rate constant, $k_{\text{eff}} = 7.3 \pm 1.9 \times 10^{-3} \text{ min}^{-1}$.

between Mn^{II} and Mn^{III} sites) within nano-crystalline (~10 nm) Mn₃O₄ (0.45–0.69 eV),⁵¹ and suggests that the slow step for manganese etching is an interfacial electron transfer event:



where the manganese impurities remain in the solid state, during inner-sphere oxidation⁵² by hypochlorite ions across the solid/liquid interface.

In order to confirm the dissolution rate as being controlled by an interfacial electron transfer process, ambient temperature experiments were undertaken in which the chemical oxidant was replaced by distilled water saturated with both ozone and lime hydrate (pH 12.3). In this case (data not shown), the value of k_{het} was observed to be $2.2 \pm 0.1 \times 10^{-8} \text{ mol min}^{-1}$ (when corrected for the greater solubility of lime hydrate in water than in sodium hydroxide solution). This value is significantly larger than that observed at ambient temperature for alkaline hypochlorite oxidants, even after accounting for the concentration differences⁵³ between ozone (at saturation, ~5 mM) and the hypochlorite solution used (~2.5 M). Nevertheless, these results are consistent with the expected linear free energy nature of the activation/driving force within the normal Marcus region;⁵⁴ the standard potentials at^{45a} pH 14, $E_B^0 = +1.24 \text{ V vs. SHE}$ (for O₃/O₂), with $E_B^0 = +0.89 \text{ V vs. SHE}$ (for ClO⁻/Cl⁻) confirm the greater oxidising strength of ozone compared with hypochlorite, and, thence, the faster dissolution rate in the presence of ozone.

The observation of zeroth-order kinetics for manganese loss from slaked lime gives rise to a “rule-of-thumb” for the scale-up of this process chemistry. However, it is important to realise that after removal of *ca.* 75% of the original manganese impurity, a constant amount remains, as determined *via* ICP-OES (Fig. 9). This is “inactive” manganese – it is inaccessible and cannot be removed through a chemical etch with

hypochlorite – either because it is too deep within the core of the hydrate particles (within the 3% calcite), or because it is in a different “shell” of the hydrate, or even in a different oxidation form, compared with the “active manganese”, and thus has a slower etching rate constant.

We next consider how the insights into this chemical etching chemistry can be adapted to existing processes where lime is used for the drinking water distribution network.

Adaptation for end-use

Current methods for the removal of soluble iron and manganese in drinking water typically uses elaborate filtration beds, each with a unit treatment cost of €0.12 m⁻³ (for a mid-sized water treatment plant).⁹ The removal of iron or manganese in drinking water treatment chemicals is not a standard practice, so that implementation of corrective actions, such as those indicated herein, necessarily has to be of low cost. Given this, considering typical water treatment plants employ pH modifiers such as lime, and oxidative disinfection chemicals such as chlorine or hypochlorite at a number of process stages, “manganese-free” lime is only needed if there is no filtration bed after the last combination of lime and oxidant. This reduces the demand for “manganese-free” lime.

The chemical etching pathway demonstrated herein suffers from slow, zeroth-order heterogeneous kinetics, and this requires process heat to raise the temperature to 90 °C. However, these high temperatures facilitate the decomposition of the alkaline oxidant required, so that a cascade approach is required, if hypochlorite is used as the oxidant, which adds to the overall operational expenditure required: this work has demonstrated capability only using at a solid hydrate to liquid solution oxidant ratio of between 0.0125–0.025 g mL⁻¹. Whilst further work may be able to demonstrate viability through increasing this ratio, an alternative is to employ the use of a



different oxidant, such as the continual bubbling of chlorine gas in an aqueous lime slurry (“aqualime”). Although lime manufacturers do distribute aqualime, they tend not to have chlorine gas on-site. However, water treatment plants typically have opportunities to make aqualime on-plant, and sometimes may have the process safety infrastructure needed to use chlorine on-plant, so that water companies may use this chemistry. An additional advantage of performing this chemistry on a water treatment plant is that the permanganate and ferrate generated can be used to remove the odour associated with reduced gases (such as hydrogen sulphide and ammonia) that are typically present on such sites.

Conclusions

In this work, we have developed high pH redox chemistry that demonstrates how both manganese and iron impurities can be removed from lime hydrate derived from quarried limestones. The mechanism for the oxidative removal is different for both iron and manganese: in the former, oxygenated solutions are required to transform the surface ferric oxide into ferrite, which can be solubilised through oxidation with hypochlorite to yield soluble ferrate; in contrast, hausmannite is oxidised stepwise by hypochlorite (or ozone), ultimately to furnish soluble permanganate.

These reactions are under activation control, with the kinetics of oxidation increasing with temperature. For manganese, these dissolution kinetics are zeroth-order that appear to be limited by the rate of electron transfer, enabling design rules for the up-scale of this process to be determined of $\sim 1\% \text{ min}^{-1}$ for manganese and $\sim 3\% \text{ min}^{-1}$ for iron, at 90 °C. However, it is important to realise that this chemistry cannot create a completely “manganese-free” or “iron-free” product: around 25% of the total manganese (“inactive” manganese) remains, irrespective of the feedstock (Carboniferous limestone or Cretaceous chalk).

Although further work is needed to examine the economic viability of this process chemistry at scale, it nevertheless provides an opportunity for manufacturers to develop suitable lime hydrate products that hold very low levels of manganese and iron impurities. Alternatively, given the simplicity of the operations, and that the treatment chemicals are similar to those already deployed for disinfection in the water industry, the impurity-removal process could potentially be integrated on the site of existing water treatment works.

Last, we note that control of manganese in lime products is important for processes other than in those employed by the water industry.^{55–57}

Author contributions

Conceptualisation: DK, CRM, NSL, JDW. Methodology: DK, CRM, NSL, JDW. Investigation: DK. Formal analysis: DK, CRM, NSL, JDW. Software: DK, JDW. Validation: DK, RAW. ICP-OES: MT. X-Ray diffraction and analysis: TJP. Resources: DK, CRM, SMK, NSL, JDW. Data curation: DK, CRM, JDW.

Writing – original draft: DK, CRM, NSL, JDW. Writing – review and editing: DK, RAW, CRM, MT, TJP, SMK, NSL, JDW. Visualisation: DK, CRM, NSL, JDW. Supervision: DK, CRM, NSL, JDW. Project administration: CRM, NSL, JDW. Funding acquisition: CRM, SMK, NSL, JDW.

Conflicts of interest

DK and CRM are both employed by Singleton Birch Ltd.

Acknowledgements

This work was funded by Singleton Birch Ltd. (50%), together with InnovateUK (25%) and the Engineering and Physical Sciences Research Council (25%), through a Knowledge Transfer Partnership (Programme Number 0110770). DK thanks The University of Hull for funding his MSc research studentship. RAW thanks Singleton Birch for funding. We thank Haydn Ward (ParagonID) for the generous donation of both magnetite and maghaemite used in this work, Pauline Smedley (British Geological Survey) for arranging access to ref. S25,† and Bernadette Ryan (Severn Trent, Plc) and Anna Taliana (Dŵr Cymru Welsh Water) for useful discussions. DK, NSL and JDW thank the Johnston Quarry Group for generously supplying a sample of Great Tew Ironstone. We are grateful to two anonymous reviewers who have improved the flow of this manuscript.

Notes and references

- 1 See, for example, United Nations General Assembly Resolution 64/292, *The Human Right to Water and Sanitation*, United Nations, adopted July 28, 2010.
- 2 E. C. Craig, E. L. Bean and R. W. Sawyer, Iron and lime in removal of manganese, *J. - Am. Water Works Assoc.*, 1932, 24, 1762.
- 3 The complexity of the water distribution and regulatory framework in the United Kingdom is elegantly captured in a recent speech by Sir James Bevan, Chief Executive of the Environment Agency, *Escaping the Jaws of Death: Ensuring Enough Water in 2050*, Waterwise Conference, March 19, 2019, full transcript available at the following URL, <https://www.gov.uk/government/speeches/escaping-the-jaws-of-death-ensuring-enough-water-in-2050>, (Accessed December 28, 2021).
- 4 World Health Organisation, *Guidelines for Drinking Water Quality*, World Health Organisation, Geneva, 4th edn, (incl. 1st add.), 2017.
- 5 See, for example, D. K. Todd and L. W. Mays, *Groundwater Hydrology*, Wiley, New Delhi, 3rd edn, 2005.
- 6 (a) For example, the chalk aquifer of the East Riding of Yorkshire is contaminated by both atrazine (a pesticide) and dichloromethane (a non-aqueous phase liquid) at concentrations above European guideline values, *q.v.*, I. N. Gale and H. K. Rutter, *The Chalk Aquifer of Yorkshire*, British Geological Survey Research Report RR/06/04, British Geological Survey, Keyworth, 2006; (b) Likewise, “forever



chemicals" such as perfluorinated hydrotopes have been found in soils, surface waters and groundwaters throughout England: see, for example, E. Pemberton, *Poly- and Perfluoroalkyl Substances (PFAS): Sources, Pathways and Environmental Data*, Chief Scientist's Report, Environment Agency, Bristol, 2021.

7 (a) J. Fawell and M. J. Nieuwenhuijsen, Contaminants in drinking water, *Br. Med. Bull.*, 2003, **68**, 199; (b) S. Sharma and A. Bhattacharya, Drinking water contamination and treatment techniques, *Appl. Water Sci.*, 2017, **7**, 1043.

8 (a) S. Zahran, D. Mushinski, S. P. McElmurry and C. Keyes, Water lead exposure risk in Flint, Michigan after switchback in water source: implications for lead service line replacement policy, *Environ. Res.*, 2020, **181**, 108928; (b) K. J. Pieper, M. Tang and M. A. Edwards, Flint water crisis caused by interrupted corrosion control: investigating "ground zero" home, *Environ. Sci. Technol.*, 2017, **51**, 2007.

9 *Best Practice Guide on the Control of Iron and Manganese in Water Supply*, ed. A. Postawa and C. Hayes, IWA Publishing, London, 2013.

10 Drinking Water Inspectorate, *Drinking Water 2020: The Chief Inspector's Report for Drinking Water in England*, Drinking Water Inspectorate, London, 2021.

11 (a) V. A. Pattinson, D. P. Butcher, J. C. Labadz and J. Shacklock, Water discolouration and the ô of the reservoir, *Phys. Chem. Earth*, 1995, **20**, 175; (b) S. Buss, *Review of Spatial Factors Controlling Water Discolouration in England and Wales*, Appendix 10, Technical Note 64116BN TN1D1, ESI, Ltd., 2018.

12 (a) L. I. Sly, M. C. Hodgkinson and V. Arunpairojana, Deposition of manganese in a drinking water distribution system, *Appl. Environ. Microbiol.*, 1990, **56**, 628; (b) J. M. Cerrato, L. P. Reyes, C. N. Alvarado and A. M. Dietrich, Effect of PVC and iron materials on Mn(II) deposition in drinking water distribution systems, *Water Res.*, 2006, **40**, 2720; (c) J. H. H. Vreeburg and J. B. Boxall, Discolouration in potable water distribution systems: a review, *Water Res.*, 2007, **41**, 519.

13 (a) For a thorough discussion of process improvements suggested by Severn Trent to improve their distribution of soft water, derived from the Elan Valley catchment in Wales, to the City of Birmingham (maximum flow of 450 ml per day), so as to reduce the iron, manganese, colour, turbidity and natural aluminium levels, see T. Schofield, R. Perkins and J. S. Simms, Frankley Water Treatment Works redevelopment: pilot-scale studies, *Water Environ. J.*, 1991, **5**, 370; (b) A. E. Griffin, Significance and removal of manganese in water supplies, *J. - Am. Water Works Assoc.*, 1960, **52**, 1326.

14 S.-W. Lee, M. Jones, C. Romano and B. M. Tebo, Formation of manganese oxide minerals by bacteria, in *Redox-Reactive Minerals: Properties, Reactions and Applications in Natural Systems and Clean Technologies*, ed. I. A. M. Ahmed and K. A. Hudson-Edwards, EMU Notes in Mineralogy, The Mineralogical Society of Great Britain and Ireland, London, 2017, ch. 7, vol. 17, p. 173.

15 D. Dixon, N. Anderson, B. Bolto, B. Chiswell, L. Sly, T. Hurse, K. Craig, G. Hamilton, B. Hutchinson, C. West and R. Woolley, *The Removal of Manganese from Drinking Waters*, Research Report No. 26, The Co-operative Research Centre for Water Quality and Treatment, Salisbury, Australia, 2006.

16 (a) We note that recent laboratory-scale research^{16b} has illustrated how Mn²⁺ (at concentrations of 2 ppm in 0.1 M aqueous phosphate buffer) can be removed as Mn₂O₃ (lowering the aqueous concentration to ca. 900 ppb) via advanced electrochemical oxidation, although this technology has yet to be assessed for technical, environmental and economic feasibility; (b) S. T. McBeath, D. P. Wilkinson and N. J. D. Graham, Advanced electrochemical oxidation for the simultaneous removal of manganese and generation of permanganate oxidant, *Environ. Sci.: Water Res. Technol.*, 2020, **6**, 2405.

17 (a) G. Dillon, P. Jackson, A. Ewence and J. Jonsson, *Potential Contaminants in Drinking Water Treatment Chemicals: Final Report to the Department for the Environment, Food and Rural Affairs*, Report No. Defra9033.03, WRc, plc, Swindon, 2003; (b) Note that in the USA, similar standards are in operation, see NSF/ANSI 60-2016, *Drinking Water Treatment Chemicals – Health Effects*, NSF International, Michigan, 2016; (c) P. Rumsby, H. Clegg, J. Jonsson, V. Benson, M. Harman, T. Doyle, L. Rushton, P. Warwick and D. Wilkinson, *Speciation of Manganese in Drinking Water: Final Report for the Drinking Water Inspectorate*, Report No. DWI70-2-276, WRc, plc, Swindon, 2014.

18 (a) S. R. Jenkins, L. Benefield, M. J. Keal and R. S. Peacock, Effective manganese removal using lime as an additive, *J. - Am. Water Works Assoc.*, 1984, **76**, 82; (b) A. M. Silva, F. L. S. Cruz, R. M. F. Lima, M. C. Teixeira and V. A. Leão, Manganese and limestone interactions during minewater treatment, *J. Hazard. Mater.*, 2010, **181**, 514; (c) D. L. Trollip, J. C. Hughes and L. W. Titshall, Sources of manganese in the residue from a water treatment plant, *Water SA*, 2013, **39**, 265.

19 (a) A. Hamdouni, G. Montes-Hernandez, M. Tlili, N. Findling, F. Renard and C. V. Putnis, Removal of Fe(II) from groundwater via aqueous portlandite carbonation and calcite-solution interactions, *Chem. Eng. J.*, 2016, **283**, 404; (b) A. Sdiri, T. Higashi, T. Hatta, F. Jamoussi and N. Tase, Removal of heavy metals from aqueous solution by limestone, *Int. J. Glob. Environ. Issues*, 2012, **12**, 171; (c) B. I. Whittington, The chemistry of CaO and Ca(OH)₂ relating to the Bayer process, *Hydrometallurgy*, 1996, **43**, 13.

20 (a) S. Caserini, N. Storni and M. Grossi, The availability of limestone and other raw materials for ocean alkalinity enhancement, *Global Biogeochem. Cycles*, 2022, **36**, e2021GB007246; (b) J. Hartmann and N. Moosdorf, The new global lithological map database GLiM: a representation of rock properties at the Earth surface, *Geochem., Geophys., Geosyst.*, 2012, **13**, 1.

21 (a) Data taken from (i) *USGS Mineral Commodity Summaries 2022*, U.S. Geological Survey, Reston, Virginia, 2022, and (ii) the associated data release for the 2020 tables, available to download at <https://www.usgs.gov/centers/national-minerals-information-center/lime-statistics-and-information>, accessed



January 6, 2023; (b) This is in agreement with the proportion of end-use of ground calcium carbonate (9%) used for environmental protection (flue gas, drinking water and sewage treatment) reported in European Commission, *Report on Critical Raw Materials for the EU: Non-Critical Raw Materials Profiles*, 2014, Reference: Ares(2014)3690319-06/11/2014.

22 (a) Department of the Environment, *Appraisal of High-Purity Limestones in England and Wales: A Study of Resources, Needs, Uses and Demands: Summary Report*, Department of the Environment, London, 1990; (b) D. J. Harrison, J. M. Hudson and B. Cannell, *Appraisal of High-Purity Limestones in England and Wales: A Study of Resources, Needs, Uses and Demands: Part 1: Resources*, British Geological Survey Mineral Resources Series WF/90/10, British Geological Survey, Keyworth, 1991; (c) D. J. Harrison, High-purity limestones in England and Wales, *Q. J. Eng. Geol.*, 1993, **26**, 293; (d) D. J. Harrison, D. Highley, A. Bloodworth, R. Bate, D. Cameron, P. Lusty and D. Rayner, *Limestone*, Mineral Planning Factsheet prepared for the Office of the Deputy Prime Minister, British Geological Survey, Keyworth, 2006, available to download from <https://www.mineralsUK.com>, (accessed December 28, 2021); (e) C. Mitchell, High-purity limestone quest, *Ind. Miner.*, 2011, 48.

23 The British Lime Association (one of the constituent bodies of the Mineral Products Association) is the trade organisation for the companies that are responsible for producing at least 75% (ca. 1.2 MTe y^{-1}) of the industrial lime sold in the UK: <https://www.britishlime.org> (accessed December 28, 2021). The British Calcium Carbonate Federation is the trade body representing the interests of UK producers and suppliers of chalk, limestone, marble, dolomite and precipitated calcium carbonate, whose members produce >3.5 MTe y^{-1} of calcium carbonate products: <https://www.calciumcarbonate.org.uk>, (accessed December 28, 2021).

24 (a) G. D. Gaunt, T. P. Fletcher and C. J. Wood, *Geology of the Country Around Kingston-upon-Hull and Brigg: Memoir for 1:50000 geological sheets 80 and 89 (England and Wales)*, British Geological Survey, Her Majesty's Stationery Office, London, 1992; (b) F. Whitham, The geology of the Melton Ross chalk quarries, *Humber Geologist*, No. 12, Hull Geological Society, Kingston-upon-Hull, 1999, available online: <https://www.hullgeolsoc.co.uk/meltonrs.htm>, (accessed December 28, 2021).

25 (a) D. J. Harrison, *The Limestone and Dolomite Resources of the Country Around Buxton, Derbyshire: Description of 1:25000 sheet SK 07 and parts of SK 06 and 08*, Mineral Assessment Report 77 for the Institute of Geological Sciences, Her Majesty's Stationery Office, London, 1981; (b) D. J. Harrison and K. A. McL. Adlam, *Limestones of the Peak: A Guide to the Limestone and Dolomite Resources of the Peak District of Derbyshire and Staffordshire: Description of parts of 1:50000 geological sheets 99, 111, 112, 124 and 125*, Mineral Assessment Report 144 for the British Geological Survey, Her Majesty's Stationery Office, London, 1985.

26 (a) F. C. Cox, D. McC. Bridge and J. H. Hull, *Procedure for the Assessment of Limestone Resources*, Mineral Assessment Report for the Institute of Geological Sciences, No. 30, Her Majesty's Stationery Office, London, 1977; (b) D. J. Harrison, *Industrial Minerals Laboratory Manual: Limestone*, Mineralogy and Petrology Series Technical Report WG/92/29, British Geological Survey, Keyworth, 1993; (c) D. J. Harrison, S. D. J. Inglethorpe, C. J. Mitchell, S. J. Kemp, P. Chaodumrong and M. Charusribandhu, *Procedures for the Rapid Assessment of Limestone Resources*, Overseas Geology Series Technical Report WC/98/1, British Geological Survey, Keyworth, 1998.

27 R. S. Boynton, *Chemistry and Technology of Lime and Limestone*, John Wiley and Sons, New York, 2nd edn, 1980.

28 (a) W. M. Edmunds, W. G. Darling, D. G. Kinniburgh, L. Dever and P. Vachier, *Chalk Groundwater in England and France: Hydrogeochemistry and Water Quality*, British Geological Survey Research Report SD/92/2, Keyworth, 1992; (b) Whilst limestone rocks are generally known to give rise to karstland that characterised geomorphological features including caves, sink holes and dolines, the non-karstic nature of chalk landscapes has been challenged recently – see L. Maurice, A. R. Farrant, E. Mathewson and T. Atkinson, Karst hydrogeology of the Chalk and implications for groundwater protection, in *The Chalk Aquifers of Northern Europe*, ed. R. P. Farrell, N. Massei, A. E. Foley, P. R. Howlett and J. J. West, Geological Society Special Publications, Geological Society, London, 2023, vol. 517, in press: DOI: [10.1144/SP517-2020-267](https://doi.org/10.1144/SP517-2020-267).

29 P. Shand and J. Bloomfield, *Mineralisation of Shallow Fracture Surfaces in the Chalk and Implications for Contaminant Attenuation*, British Geological Survey Hydrology Series Technical Report WD/95/15, British Geological Survey, Keyworth, 1995.

30 I. Casas, D. Casabona, L. Duro and J. de Pablo, The influence of haematite on the sorption of uranium(VI) onto granite filling fractures, *Chem. Geol.*, 1994, **113**, 319.

31 O. Landström and E. L. Tulborg, *The Influence of Fracture Mineral/Groundwater Interaction on the Mobility of U, Th, REE and Other Trace Elements*, SKB (Swed. Nucl. Fuel & Waste Manage. Co.), Technical Report 90-37, Stockholm, 1990.

32 K. A. Hudson-Edwards and D. Kossoff, Rôle of redox-reactive minerals in the re-use and remediation of mine wastes, in *Redox-Reactive Minerals: Properties, Reactions and Applications in Natural Systems and Clean Technologies*, ed. I. A. M. Ahmed and K. A. Hudson-Edwards, EMU Notes in Mineralogy, The Mineralogical Society of Great Britain and Ireland, London, 2017, ch. 12, vol. 17, p. 357.

33 (a) F. C. Cox and D. Mac. Bridge, *The Limestone and Dolomite Resources of the Country Around Monyash, Derbyshire: Description of 1:25000 resource sheet SK 16*, Mineral Assessment Report 26 for the Institute of Geological Sciences, Her Majesty's Stationery Office, London, 1977; (b) P. Shand, W. M. Edmunds, A. R. Lawrence, P. L. Smedley and S. Burke, *The Natural (Baseline) Quality of Groundwater in England and Wales*, Environment Agency Technical Report NC/99/74/24, Groundwater Programme Research Report RR/07/06, British Geological Survey, Keyworth, 2007.



34 W. M. Edmunds, J. M. Cook, W. G. Darling, D. G. Kinniburgh, D. L. Miles, A. H. Bath, M. Morgan-Jones and J. N. Andrews, Baseline geochemical conditions in the Chalk aquifer, Berkshire, U.K.: a basis for groundwater quality management, *Appl. Geochem.*, 1987, **2**, 251.

35 W. R. Jones, *Minerals in Industry*, Penguin, London, 3rd edn, 1955.

36 A full range of chalk-derived lime products quarried and manufactured by Singleton Birch, Ltd., together with their physico-chemical characteristics, is available on their website: <https://www.singletonbirch.co.uk>, (accessed December 28, 2021).

37 Thermal oxidation of rhodochrosite at kiln temperatures affords hausmannite: (a) L. Biernacki and S. Pokrzynicki, The thermal decomposition of manganese carbonate: thermogravimetry and exoemission of electrons, *J. Therm. Anal. Calorim.*, 1999, **5**, 227; both bixbyite and pyrolusite likewise decompose to hausmannite under thermal kiln conditions: (b) E. Alonso, C. Hutter, M. Romero, A. Steinfeld and J. Gonzalez-Aguilar, Kinetics of Mn_2O_3 - Mn_3O_4 and Mn_3O_4 - MnO redox reactions performed under concentrated thermal radiative flux, *Energy Fuels*, 2013, **27**, 4884; (c) N. Birkner and A. Navrotksy, Thermodynamics of manganese oxides: effects of particle size and hydration on oxidation-reduction equilibria among hausmannite, bixbyite and pyrolusite, *Am. Mineral.*, 2015, **97**, 1291; the whole picture is further complicated by phase transformations: (d) A. N. Grundy, B. Hallstedt and L. J. Gauckler, Assessment of the Mn-O system, *J. Phase Equilib.*, 2003, **24**, 21.

38 Oxidation of iron pyrite at kiln temperatures affords the sesquioxide: (a) G.-M. Schwab and J. Philinis, Reactions of iron pyrite: its thermal decomposition, reduction by hydrogen and air oxidation, *J. Am. Chem. Soc.*, 1947, **69**, 2588; (b) T. Kennedy and B. T. Sturman, The oxidation of iron(II) sulphide, *J. Therm. Anal.*, 1975, **8**, 329; (c) Y. Zhang, Q. Li, X. Liu, B. Xu, Y. Yang and T. Jiang, A thermodynamic analysis on the roasting of pyrite, *Minerals*, 2019, **9**, 220; likewise, oxidation of siderite proceeds to magnetite: (d) B. M. French and P. E. Rosenberg, Siderite ($FeCO_3$): thermal decomposition in equilibrium with graphite, *Science*, 1965, **147**, 1283; and then maghemite: (e) M. Aliahmad and N. N. Moghaddam, Synthesis of maghemite (γ - Fe_2O_3) nanoparticles by thermal decomposition of magnetite (Fe_3O_4) nanoparticles, *Mater. Sci.-Pol.*, 2013, **31**, 264; (f) Note that the kiln conditions are controlled to ensure sufficient fugacity of oxygen, in a manner similar to those in the Earth: see, for example, V. Stagno and S. Aulbach, Redox processes before, during, and after Earth's accretion affecting the deep carbon cycle, in *Magma Redox Geochemistry*, ed. R. Moretti and D. R. Neuville, Wiley, Hoboken, NJ, 2022, p. 21.

39 (a) D. S. McClure, The distribution of transition metal cations in spinels, *J. Phys. Chem. Solids*, 1957, **3**, 311; (b) J. D. Dunitz and L. E. Orgel, Electronic properties of transition metal oxides II: cation distribution amongst octahedral and tetrahedral sites, *J. Phys. Chem. Solids*, 1957, **3**, 318; (c) A. H. Eschenfelder, Ionic valences in manganese-iron spinels, *J. Appl. Phys.*, 1958, **29**, 378; (d) S. K. Sahu, B. Huang, K. Lilova, B. F. Woodfield and A. Navrotksy, Thermodynamics of Fe_3O_4 - Co_3O_4 and Fe_3O_4 - Mn_3O_4 spinel solid solutions at the bulk and nanoscale, *Phys. Chem. Chem. Phys.*, 2015, **17**, 22286.

40 (a) A. T. Stone and J. J. Morgan, Reduction and dissolution of manganese(III) and manganese(IV) oxides by organics: 1: reaction with hydroquinone, *Environ. Sci. Technol.*, 1984, **18**, 450; (b) A. T. Stone, Reductive dissolution of manganese(III/IV) oxides by substituted phenols, *Environ. Sci. Technol.*, 1987, **21**, 979; (c) K. L. Johnson, C. M. McCann and C. E. Clarke, Breakdown of organic contaminants in soil by manganese oxides: a short review, in *Redox-Reactive Minerals: Properties, Reactions and Applications in Natural Systems and Clean Technologies*, ed. I. A. M. Ahmed and K. A. Hudson-Edwards, EMU Notes in Mineralogy, The Mineralogical Society of Great Britain and Ireland, London, 2017, ch. 11, vol. 17, p. 313; (d) B. Liu, Y. Zhang, M. Lu, Z. Su, G. Li and T. Jiang, Extraction and separation of manganese and iron from ferruginous manganese ores: a review, *Miner. Eng.*, 2019, **131**, 286; (e) V. Singh, S. Pati and K. Kumar, Development of a process to produce manganese nanomaterials from low grade ferruginous manganese ores, *Miner. Process. Extr. Metall.*, 2021, **130**, 324.

41 (a) S. Licht, V. Naschitz, L. Halperin, L. Lin, J. Chen, S. Ghosh and B. Liu, Analysis of ferrate(VI) compounds and super-iron Fe(VI) battery cathodes: FTIR, ICP, titimetric, XRD, UV/VIS, and electrochemical characterisation, *J. Power Sources*, 2001, **101**, 167; (b) Y. L. Wang, S. H. Ye, J. K. Bo, Y. Y. Wang and F. Wu, Electrochemical reduction mechanism of Fe(VI) at a porous Pt black electrode, *J. Electrochem. Soc.*, 2009, **156**, A572; (c) S. Barışçı, F. Ulu, H. Särkkä, A. Dimoglo and M. Sillanpää, Electrosynthesis of ferrate(VI) ion using high purity iron electrodes: optimisation of influencing parameters on the process and investigating its stability, *Int. J. Electrochem. Sci.*, 2014, **9**, 3099; (d) Y.-L. Wei, Y.-S. Wang and C.-H. Liu, Preparation of potassium ferrate from spent steel pickling liquid, *Metals*, 2015, **5**, 1770; (e) J.-Q. Jiang, C. Stanford and M. Petri, Practical application of ferrate(VI) for water and wastewater treatment – site study approach, *Water-Energy Nexus*, 2018, **1**, 42; (f) B. Shao, H. Dong and X. Guan, Rôle of ferrate(IV) and ferrate(V) in activating ferrate(VI) by calcium sulphite for enhanced oxidation of organic contaminants, *Environ. Sci. Technol.*, 2019, **53**, 894; (g) P. C. W. Cheung, D. R. Williams, J. Barrett, J. Barker and D. W. Kirk, On the origins of some spectroscopic properties of “purple iron” (the tetroxoferrate(VI) ion) and its Pourbaix safe-space, *Molecules*, 2021, **26**, 5266; (h) Note that calcium ions can catalyse the decomposition of ferrate: L. Ma, W. W. Y. Lam, P.-K. Lo, K.-C. Lau and T.-C. Lau, *Angew. Chem., Int. Ed.*, 2016, **55**, 3012.

42 See, for example, S. G. Simpson, The effect of the presence of filter paper on permanganate-oxalate titrations, *J. Ind. Eng. Chem.*, 1921, **13**, 1152.

43 (a) B. E. Dixon and J. L. White, The reaction between manganese salts and sodium hypochlorite in the presence of certain other



salts, *J. Chem. Soc.*, 1927, 1469; (b) M. Valensi, Nouvelle méthode d'enseignement de la chimie minérale, *Bull. Union Physiciens*, 1950, (394), 61; (c) *Atlas of Electrochemical Equilibria in Aqueous Solutions*, ed. M. Pourbaix, National Association of Corrosion Engineers, Houston, Texas, 2nd edn, 1974.

44 K. M. Love and A. Woronow, Chemical changes induced in aragonite using treatments for the destruction of organic material, *Chem. Geol.*, 1991, **93**, 291.

45 (a) W. M. Latimer, *The Oxidation States of the Elements and their Potentials in Aqueous Solutions*, Prentice-Hall, New York, 2nd edn, 1952; (b) K. Ishikawa, T. Yoshioka, T. Sato and A. Okuwaki, Solubility of haematite in LiOH, NaOH and KOH solutions, *Hydrometallurgy*, 1997, **45**, 129; (c) S. Uchida, T. Sato and A. Okuwaki, Formation of Na_xFeO_2 by the oxidation of iron powder in concentrated sodium hydroxide solutions at elevated temperatures, *J. Mater. Sci.*, 1995, **14**, 633.

46 (a) See, for example, B. M. Voelker and D. L. Sedlak, Iron reduction by photo-produced superoxide in seawater, *Mar. Chem.*, 1995, **50**, 93; (b) S. Garg, G. Xing and T. D. Waite, Influence of pH on the kinetics and mechanism of photo-reductive dissolution of amorphous iron oxyhydroxide in the presence of natural organic matter: implications to iron bioavailability in surface waters, *Environ. Sci. Technol.*, 2020, **54**, 6771.

47 See, for example, (a) H. P. Hopkins Jr. and C. A. Wulff, The solution thermochemistry of polyvalent electrolytes: I: calcium hydroxide, *J. Phys. Chem.*, 1965, **69**, 6; (b) W. B. Euler, L. J. Kirschenbaum and B. Ruekberg, Determination of K_{sp} , ΔG^0 , ΔH^0 and ΔS^0 , *J. Chem. Educ.*, 2000, **77**, 1039.

48 (a) J. R. Lewis, The catalytic decomposition of sodium hypochlorite solutions I: mechanism of the reaction, *J. Phys. Chem.*, 1928, **22**, 243; (b) M. W. Lister, Decomposition of sodium hypochlorite: the uncatalysed reaction, *Can. J. Chem.*, 1956, **34**, 465.

49 J. H. Atherton, Mechanism in two-phase reaction systems: coupled mass transfer and chemical reaction, in *Research in Chemical Kinetics*, ed. R. G. Compton and G. Hancock, Elsevier, Amsterdam, 1994, vol. 2, p. 193.

50 As an aside, we note that whilst calcite dissolution is typically controlled by surface kinetics – see R. G. Compton and P. R. Unwin, The dissolution of calcite in aqueous solution at $\text{pH} < 4$: kinetics and mechanism, *Philos. Trans. R. Soc., A*, 1990, **330**, 1; and R. G. Compton and K. L. Pritchard, The dissolution of calcite at $\text{pH} > 7$: kinetics and mechanism, *Philos. Trans. R. Soc., A*, 1990, **330**, 47; acidic dissolution of calcium carbonate from Southern Province Chalk has been shown to be mass transport controlled – see R. G. Compton, C. T. Walker, P. R. Unwin and W. A. House, Dissolution kinetics of Carrera Marble, Portland Stone and several limestones in acidic waters, *J. Chem. Soc., Faraday Trans.*, 1990, **86**, 849; and that different species of coccolith hold different masses of calcium carbonate *q.v.*, M. Yang, C. Batchelor-McAuley, S. Barton, R. E. M. Rickaby, H. A. Bouman and R. G. Compton, Opto-electrochemical dissolution reveals coccolith calcium carbonate content, *Angew. Chem., Int. Ed.*, 2021, **60**, 20999.

51 (a) E. M. Logothetis and K. Park, The electrical conductivity of Mn_3O_4 , *Solid State Commun.*, 1975, **16**, 909; (b) R. Metselaar, R. E. van Tol and P. Piercy, The electrical conductivity and thermoelectric power of Mn_3O_4 at high temperatures, *J. Solid State Chem.*, 1981, **38**, 335; (c) S. E. Dorris and T. O. Mason, Electrical properties and cation valencies in Mn_3O_4 , *J. Am. Ceram. Soc.*, 1988, **71**, 379; (d) H. Dhaouadi, A. Madani and F. Touati, *Mater. Lett.*, 2010, **64**, 2395; (e) V. C. Bose, K. Maniammal, G. Madhu, C. L. Veenas, A. S. A. Raj and V. Biju, *IOP Conf. Ser.: Mater. Sci. Eng.*, 2015, **73**, 012084.

52 J.-K. Wu, Kinetics of the reduction of hypochlorite ion, *J. Electrochem. Soc.*, 1987, **134**, 1462.

53 (a) A. Wilczak, W. R. Knocke, R. E. Hubel and M. E. Aieta, Manganese control during ozonation of water containing organic compounds, *J. - Am. Water Works Assoc.*, 1993, **85**, 98; (b) W. Li and S. T. Oyama, Mechanism of ozone decomposition on a manganese oxide catalyst: 2: steady-state and transient kinetic studies, *J. Am. Chem. Soc.*, 1998, **120**, 9047; (c) J. A. Roth and D. E. Sullivan, Solubility of ozone in water, *Ind. Eng. Chem. Fundam.*, 1981, **20**, 137.

54 (a) N. S. Lawrence, B. Schöllhorn and J. D. Wadhawan, Asymmetric and anharmonic electrode kinetics: evaluation of a model for electron transfer with concerted rupture of weak, inner-shell interactions, *ChemistrySelect*, 2021, **6**, 13331; (b) B. Gilbert and G. A. Waychunas, The timescale of mineral redox reactions, in *Redox-Reactive Minerals: Properties, Reactions and Applications in Natural Systems and Clean Technologies*, ed. I. A. M. Ahmed and K. A. Hudson-Edwards, EMU Notes in Mineralogy, The Mineralogical Society of Great Britain and Ireland, London, 2017, ch. 4, vol. 17, p. 55; (c) M. Sander, T. B. Hofstetter and C. A. Gorski, Electrochemical analyses of redox-active iron minerals: a review of non-mediated and mediated approaches, *Environ. Sci. Technol.*, 2015, **49**, 5862.

55 A. Lu, Y. Li, F. Liu, Y. Liu, H. Ye, Z. Zhuang, Y. Li, H. Ding and C. Wang, The photo-geochemical cycle of Mn oxides on the Earth's surface, *Mineral. Mag.*, 2021, **85**, 22.

56 S. Fraley, Manganese levels in limestone: operational issues in wet limestone flue gas scrubbing technologies, in *Lime: Building on the 100-Year Legacy of the ASTM Committee C07*, ed. M. L. Thomson and J. H. Brisch, Specialist Technical Publication, American Society for Testing and Materials, San Diego, 2012, vol. 1557, p. 167.

57 L. Lv, J. Yang, Z. Shen, Y. Zhou and J. Lu, Optimising the characteristics of calcium sulfate hydrate in the flue gas desulfurisation process: investigation of the impurities in slurry: Cl^- , Fe^{3+} and Mn^{2+} , *Chem. Ind. Chem. Eng. Q.*, 2017, **23**, 293.